

Iterative Reconstruction of SPECT Data With Adaptive Regularization

Cyril Riddell, Irène Buvat, Annarita Savi, Maria-Carla Gilardi, and Ferruccio Fazio

Abstract—A nonlinear regularizing least-square reconstruction criterion is proposed for simultaneously estimating a single-photon emission computed tomography (SPECT) emission distribution corrected for attenuation together with its degree of regularization. Only a regularization trend has to be defined and tuned once for all on a reference study. Given this regularization trend, the precise regularization weight, which is usually fixed *a priori*, is automatically computed for each data set to adapt to the noise content of the data. We demonstrate that this adaptive process yields better results when the noise conditions change than when the regularization weight is kept constant. This adaptation is illustrated on simulated cardiac data for noise variations due to changes in the acquisition duration, background intensity, and attenuation map.

Index Terms—Attenuation, biomedical image processing, image reconstruction, inverse problems, regularization, single photon emission computed tomography (SPECT).

I. INTRODUCTION

TODAY'S single photon emission computed tomography (SPECT) tomographs are multiheaded devices equipped with a transmission source that allow for the measurement of the emission distribution of a patient together with its attenuation characteristics [1]–[3]. Attenuation correction can thus be performed, which is essential to the quantification of SPECT studies [4]–[6]. Iterative algorithms are compulsory for reconstructing images from SPECT data with the aim of quantification using attenuation correction [7]. Iterative methods present some drawbacks such as the noise amplification as the number of iterations increases. To prevent large noise amplification, regularization is often used, and the resulting solution is then a tradeoff between fidelity to the measured data and bias due to the regularity of the solution constrained through the regularization term [8]. This implies that a regularization parameter is set *a priori*, in a way that optimizes this tradeoff for a given situation. This regularization parameter may then be kept unchanged for all the patients enrolled in a given protocol, considering that conditions do not differ much from one study to another. This is only partially true, since activity distribution and noise characteristics do vary amongst patients. According to the size and physiology of the patient, the tracer uptake will vary in the target

organ, as well as in the peripheral organ (such as the liver in cardiac studies), which may generate additional background noise for constant acquisition conditions. The total duration of a scan can be adjusted to compensate for change in patient size, but this results in variation of the acquisition conditions themselves.

In the following study, we describe a technique for simultaneously estimating the regularized least-square solution of a SPECT reconstruction problem together with its degree of regularization to automatically find an appropriate tradeoff between noise and bias as the noise in the data changes. This adaptation is illustrated on simulated cardiac data for noise variations due to changes in the acquisition duration, background intensity, and attenuation map, as can be encountered in clinical practice.

II. THEORY

An image is estimated from a finite set of SPECT attenuated measurements by solving a linear system such as

$$R_a f = s \quad (1)$$

where f is the unknown activity distribution, s is the attenuated SPECT sinogram, and R_a is a matrix that models a SPECT tomographic acquisition with nonuniform attenuation. In this work, we propose a *nonlinear* regularizing least-square approach that builds upon the following normal equations:

$$T^t D T x = T^t D s \quad (2)$$

where $T = R_a \Gamma$ is the discretized attenuated Radon transform R_a normalized by the Chang correction Γ [9], while D stands for the ramp filtering operation. The symbol T^t denotes the transpose matrix of T . Vector x is an intermediate unknown image vector that is defined such that $f = \Gamma x$, to preserve the system symmetry. The ramp filter and the Chang correction are used as a preliminary approximate inversion making the matrix $T^t D T$ close to the identity matrix, in order to speed convergence up and work with normalized operators [10], [11]. Equation (2) leads to the following linear least-square minimization problem:

$$\min_x \left\{ \varphi(x) = \left\| D^{1/2} (T x - s) \right\|^2 \right\}. \quad (3)$$

A regularization term $\rho(x)$ is added to avoid noise amplification by constraining the norm of the image gradient ∇x

$$\rho(x) = \|\nabla x\|^2 = \langle \Delta x, x \rangle \quad (4)$$

Manuscript received November 25, 2001.

C. Riddell was with the U494 INSERM, CHU Pitié-Salpêtrière, Paris, France and GE-SMVI, Buc, France. He is now with GE Medical Systems Europe, Buc, France (e-mail: cyril.riddell@med.ge.com).

I. Buvat is with the U494 INSERM, CHU Pitié-Salpêtrière, Paris, France (e-mail: buvat@imed.jussieu.fr).

A. Savi, M.-C. Gilardi, and F. Fazio are with INB-CNR—Consiglio Nazionale delle Ricerche, Università di Milano—Bicocca, Istituto H. S. Raffaele, Milan 20090, Italy.

Digital Object Identifier 10.1109/TNS.2002.803677

where Δ stands for the normalized Laplacian operator and $\langle \cdot, \cdot \rangle$ stands for the dot product. The following regularizing least-square functional is obtained:

$$M(x) = \varphi(x) + \alpha\rho(x). \quad (5)$$

For a given strictly positive α , this functional has a unique minimum that is a compromise between fidelity to the data [the term $\varphi(x)$] and regularity of the solution [the term $\rho(x)$]. Kang and Katsaggelos have shown that it is possible to simultaneously estimate an image and its degree of regularization by making an explicit dependence between them [12]. The simultaneous estimation is obtained by finding the minimum of

$$M(x, \alpha(x)) = \varphi(x) + \alpha(x)\rho(x) \quad (6)$$

under the constraint of a *linear* relationship between the regularization parameter and the regularizing functional

$$\alpha(x) = \gamma M(x, \alpha(x)). \quad (7)$$

By so doing, $\alpha(x)$ is made proportional to $\varphi(x)$ and $\rho(x)$, which both increase with the noise in the data. The value of γ can be set such that the function $\alpha(x)$ is monotonically increasing, mapping \mathbf{R}^n into $[0, +\infty[$ and such that the functional M is convex with a unique minimum.

The minimum of M with respect to α coincides with the minimum of M with respect to x and is found by solving

$$\begin{cases} T^t D T x + \alpha(x) \Delta x = T^t D s \\ \alpha(x) = \frac{\varphi(x)}{(\frac{1}{\gamma} - \rho(x))} \end{cases}. \quad (8)$$

This system can be solved with a successive approximation scheme [12]. However, much faster convergence is obtained when using the conjugate gradient algorithm. To apply the conjugate gradient to this nonlinear problem, $\alpha(x)$ is estimated at each iteration but changed only if the new estimate of α is different enough from its current value. When $\alpha(x)$ is updated, the conjugate gradient is restarted from the current estimate of the distribution to solve the system defined by the new value of α . A similar trick was used by Kaufman for applying a positivity constraint with the conjugate gradient [13].

In this approach, the regularization strength α is modulated by the value of γ that we call the regularization “trend” in the following. Our strategy involves setting this regularization trend γ so that the algorithm produces a given regularization strength α for a reference study, for which this regularization strength is optimized. Then, solving system (8) must produce a decreased or increased regularization strength when the acquisition conditions are improved or degraded while γ is left unchanged. In order to keep γ constant, whatever the true activity distribution $f^* = \Gamma x^*$, γ must be normalized by $\|x^*\|^2$. Since the true distribution is unknown, the norm $\|x^*\|^2$ is estimated by

$$\langle x^*, x^* \rangle \approx \langle T^t D T x^*, x^* \rangle = \langle D s, s \rangle. \quad (9)$$

III. EXPERIMENTS

A segmented computed tomography (CT) slice from the Zubal phantom at the heart level was considered [14]. The simulated activity distribution was obtained by setting the heart muscle to 10 counts/s, the blood pool to 3 counts/s, the lungs to

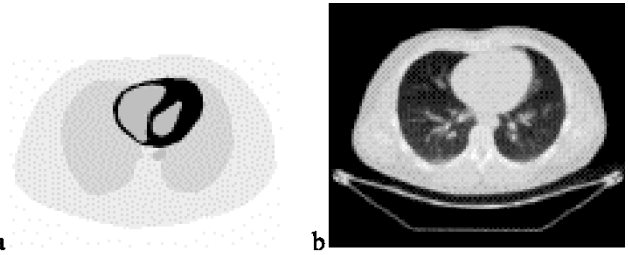


Fig. 1. (a) Emission and (b) transmission images used for the simulation of SPECT data.

2 counts/s, while all other tissues were merged into a uniform background set to 1 [Fig. 1(a)]. The image was projected in parallel geometry over 360° with 120 steps (bin size 4 mm), by taking attenuation into account. The attenuation map was taken as the nonsegmented CT slice ([Fig. 1(b)] scaled to mimic attenuation undergone by Tc^{99m} photons (attenuation of 0.15 cm^{-1} in water) and by Tl^{201} photons (attenuation of 0.17 cm^{-1} in water). With Tc^{99m} , the total activity in the sinogram was equal to 2675 counts/s. Four levels of noise were considered, corresponding to acquisition times of 50, 100, 200, and 500 s. Two additional variations were introduced with Tc^{99m} data to mimic variations of uptake in peripheral organs: 1) background and lung values were zeroed and 2) background and lung values of the original distribution were doubled. In total, 16 configurations were thus considered (three activity distributions \times four acquisition durations for Tc^{99m} , four acquisition durations for Tl^{201}) to study the robustness of the regularization trend determined from one activity distribution and then applied to different ones.

Given the known emission distribution f^* , noise and bias in a reconstructed image f' were characterized by calculating the normalized mean-square error (NMSE) between the estimated activity distribution and the true activity distribution

$$\varepsilon = 10\,000 \cdot \frac{\|f' - f^*\|^2}{\|f^*\|^2}. \quad (10)$$

Two regularization approaches were compared: fixed regularization (FR), i.e., the conjugate gradient applied to (5), and adaptive regularization (AR), i.e., the conjugate gradient applied to (8).

For a given data set, $\varepsilon(\alpha)$ could be calculated using the conjugate gradient with FR. On the other hand, AR automatically determined $\varepsilon(\alpha)$ for any data set, once γ was fixed. To set the regularization trend, a particular configuration was considered, corresponding to a 100-s acquisition time with the Tc^{99m} attenuation map and the nonspecific activity consisting of two in the lungs and one in the background. For this study, the α value minimizing the NMSE between the estimated activity distribution and the true activity distribution was found equal to 0.99. The corresponding γ was deduced and was equal to 3.0. This fixed γ was then kept to process all other 15 configurations, leading to a different α value for each configuration.

For all 16 data sets, we computed the NMSE error of the solution generated by AR, and compared this error to the lowest NMSE as obtained using the conjugate gradient with FR with α varying by steps of 0.1.

TABLE I
AR FOR Tc^{99m} ATTENUATED DATA, WITH A BACKGROUND VALUE
OF ONE AND LUNG VALUES OF TWO

Acq. duration	α_{AR}	ε_{AR}	ε^*	$\frac{(\varepsilon_{AR}-\varepsilon^*)}{\varepsilon^*}$	$\frac{(\varepsilon_{FR}-\varepsilon^*)}{\varepsilon^*}$
50	1.42	867	861	1%	8%
100	0.99	652	652	0%	0%
200	0.63	532	532	0%	3%
500	0.36	365	365	0%	27%

TABLE II
AR FOR Tl^{201} ATTENUATED DATA, WITH A BACKGROUND VALUE
OF ONE AND LUNG VALUES OF TWO

Acq. duration	α_{AR}	ε_{AR}	ε^*	$\frac{(\varepsilon_{AR}-\varepsilon^*)}{\varepsilon^*}$	$\frac{(\varepsilon_{FR}-\varepsilon^*)}{\varepsilon^*}$
50	1.54	942	928	2%	9%
100	1.10	717	710	1%	3%
200	0.74	596	593	0%	1%
500	0.40	436	436	0%	15%

IV. RESULTS

Tables I–IV show the performances of adaptive regularization for $\gamma = 3.0$: for all acquisition times (first column), the regularization values α_{AR} obtained by solving system (8) with the conjugate gradient are given in the second column together with the corresponding NMSE, denoted ε_{AR} , in the third column. FR was used to find the lowest NMSE, denoted ε^* , that is given in the fourth column. The NMSE that would be obtained if α were kept fixed to 0.99 whatever the data set is denoted ε_{FR} . The last two columns indicate the respective performances of AR and FR by giving the percentage difference between the automatically found ε_{AR} value and the optimal ε^* , and between the NMSE ε_{FR} corresponding to the fixed regularization parameter and the optimal ε^* .

Convergence was obtained after 15 iterations of the conjugate gradient with both fixed and adaptive regularization (curves not shown).

Table I shows the results obtained with the Tc^{99m} attenuated data with a background value of one and lung values of two. As expected, AR increased the regularization parameter for the acquisition duration of 50 s that was shorter than that used for optimizing γ (the data set used for the optimization was 100 s in duration). On the other hand, the regularization parameter decreased when considering acquisition durations greater than 100 s as the data got less noisy. For all acquisition times, the NMSE corresponding to the regularization parameter automatically found using AR was very close to the smallest NMSE that could be found by manually optimizing α . AR yielded regularization values more than four times higher for the shortest acquisition duration compared to the longest acquisition duration. When keeping the regularization value of 0.99 constant for all data sets, the resulting NMSE was higher than the optimal NMSE by as much as 27%.

Table II illustrates the automatic changes in α for changes in the simulated data sets induced by considering the attenuation map corresponding to Tl^{201} instead of Tc^{99m} . As photons emitted by Tl^{201} are more attenuated by the human body than photons emitted by Tc^{99m} , the Tl^{201} data were noisier than the Tc^{99m} data for the same acquisition duration. Therefore, an in-

TABLE III
AR FOR Tc^{99m} ATTENUATED DATA, WITH BACKGROUND
AND LUNG VALUES EQUAL TO ZERO

Acq. duration	α_{AR}	ε_{AR}	ε^*	$\frac{(\varepsilon_{AR}-\varepsilon^*)}{\varepsilon^*}$	$\frac{(\varepsilon_{FR}-\varepsilon^*)}{\varepsilon^*}$
50	1.02	854	834	2%	1%
100	0.66	719	703	2%	10%
200	0.41	564	552	9%	29%
500	0.27	417	381	9%	76%

TABLE IV
AR FOR Tc^{99m} ATTENUATED DATA, WITH BACKGROUND VALUE
OF TWO AND LUNG VALUES OF FOUR

Acq. duration	α_{AR}	ε_{AR}	ε^*	$\frac{(\varepsilon_{AR}-\varepsilon^*)}{\varepsilon^*}$	$\frac{(\varepsilon_{FR}-\varepsilon^*)}{\varepsilon^*}$
50	1.21	626	555	13%	20%
100	0.82	480	450	7%	3%
200	0.51	399	369	8%	0%
500	0.30	297	286	4%	12%

crease of the regularization values was expected compared to those obtained for Tc^{99m} (Table I), for the same acquisition durations. Table II demonstrates this behavior, with regularization values varying from 0.40 to 1.54 for 500–50 s acquisition durations for Tl^{201} data, to be compared with regularization values varying from 0.36 to 1.42 for Tc^{99m} . NMSE were within 2% of the lowest NMSE in each case, whereas when using fixed regularization, NMSE greater than the lowest NMSE by up to 15% were observed.

Table III shows the performance of AR for Tc^{99m} attenuated data when background and lung values were set to zero while they were different from zero in the configuration used for optimizing γ . Without background, the data were less noisy as a zero background appears in the data as zeroes with a null variance. Therefore, for a given acquisition duration, the regularization parameter was expected to be smaller than for the same data including a background (Table I). This is what was actually observed, and the NMSE corresponding to the AR reconstruction were always of the same order (for the 50-s acquisition time) or smaller than those obtained using the FR reconstruction. However, the regularization value that yielded the minimum NMSE was never reached.

Table IV shows the AR results when lung and background activities were twice as much as those of the study used to calibrate the regularization trend. In that instance, AR yielded smaller regularization values than those obtained with the original background and lung activities (Table I). This is because increasing the background and lung activities changed the structures in the images, and did not simply correspond to a change of the noise in the data. However, the change in regularization value with respect to the acquisition duration was consistent. When comparing to the NMSE obtained for a fixed regularization value, AR yielded more homogeneous results for the different acquisition durations, with NMSE 4%–13% higher than the optimal NMSE, while NMSE were 0%–20% higher than the optimal NMSE with fixed regularization.

Fig. 2 displays the images corresponding to the data sets presented in Table I. The images corresponding to a regularization trend of three (second row) led to a more uniform image quality (in terms of noise in the image) for the different acquisition du-

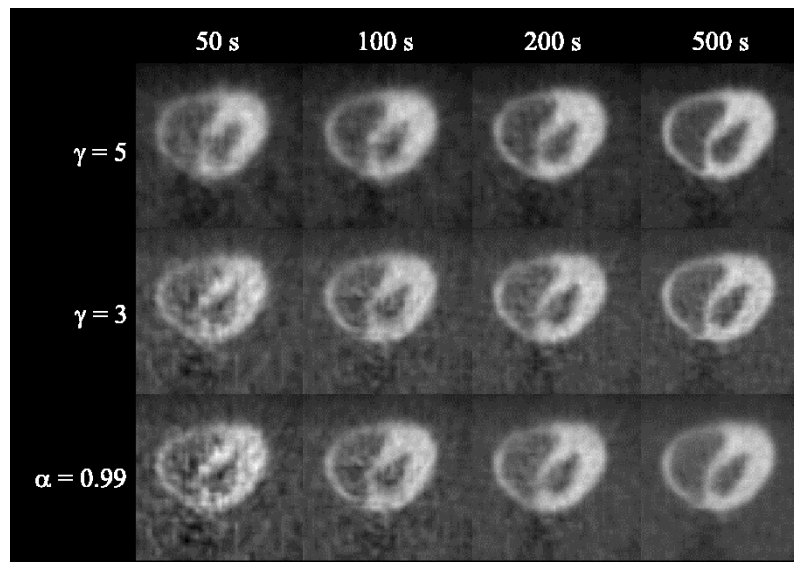


Fig. 2. Tc^{99m} attenuated data and original background and lung values. Heart muscle reconstruction with fixed regularization ($\alpha = 0.99$, bottom row) and adaptive regularization ($\gamma = 3.0$ middle row and $\gamma = 5.0$ top row).

rations than the fixed regularization (third row). The figure also illustrates that for a higher regularization trend ($\gamma = 5$, first row), even less variation in image quality was obtained for the different levels of noise in the data.

V. DISCUSSION

Adaptive regularization was demonstrated for SPECT reconstruction with attenuation correction with a nonlinear regularizing least-square criterion based on the approximate inversion of the attenuated Radon transform using the Chang correction and the ramp filter. This criterion allowed for the simultaneous estimation of the activity distribution together with its degree of regularization, according to the method proposed by Kang and Katsaggelos [12]. Images computed with fixed regularization and adaptive regularization required the same number of iterations with the conjugate gradient.

The results showed an effective regularization even though the regularization term was computed from vector x rather than from the estimate f of the distribution (4). This is because the Chang correction essentially affects the low frequencies of an image.

By setting the regularization trend using a reference study, results close to optimal, in terms of NMSE, were obtained when varying the acquisition duration and the attenuation map. Even when the background intensity varied, resulting NMSE were within 9% of the minimum NMSE when zeroing the background, and within 13% when the background and lung activities were doubled.

In all cases, adaptive regularization led to more uniformity in the image quality with respect to noise changes due to variations in acquisition duration.

The proposed regularization functional sets a linear relationship between the regularization parameter and the functional itself, to make the minimization problem tractable. This linear dependency might not be strong enough to obtain a regularization parameter yielding an NMSE almost identical to the op-

timal NMSE, especially when large variations occur between two data sets (as when the background and lung activities were doubled with respect to the background and lung values of the reference study). There might be other relationships that adapt more precisely to such variations.

Further work is needed to see if this adaptive technique can be implemented with alternative regularization constraints that can preserve the edges of the distribution, and for statistical criteria modeling Poisson noise, as in the OSEM or weighted least-square algorithms. Fessler and Rogers have already addressed the problem of normalizing the regularization constraint with respect to the weights of the criterion [15].

To demonstrate that the technique could lead to optimal noise/bias tradeoff, we used simulated data for which the true activity distribution was known. The method was shown to yield images with more uniform image quality than fixed regularization with no additional cost in terms of computation time. In the clinical context, the true distribution is unknown and the NMSE is not available. In addition, there is no direct relationship between a lower NMSE and an improved sensitivity and specificity of the diagnosis. The “best” filtering in the clinical practice often differs from a mathematical optimum. Visual inspection of Fig. 2 is, therefore, useful to convince oneself that adaptive regularization can be set based on a visual assessment only. If an observer performs better on smooth images (such as those in the first row of Fig. 2), the method will adapt to the noise content of the data to always lead to smooth images. If the noise in the data is lower than that in the reference study (acquisition duration greater than 100 s in Fig. 2), the method will yield better spatial resolution (a key factor for improving diagnosis) without the intervention of the observer. As the method also yields a regularization value that is normalized with respect to the patients, the increase or decrease of this regularization value with respect to a reference study indicates whether the data set differs in its noise content from the reference study. Further evaluation on clinical data will determine whether setting the regularization trend instead

of the regularization parameter actually reduces the variability of image quality with respect to real variations in patients physiology and anatomy, and improves the clinical interpretation of attenuation corrected SPECT images.

VI. CONCLUSION

Adaptive regularization for SPECT nonuniform attenuation correction was tested for four different acquisition durations, three background intensity levels and two attenuation conditions. By setting the regularization trend on a given reference study, the adaptive regularization decreased (or increased) the regularization strength when the acquisition duration increased (or decreased) to yield tradeoffs between noise and bias that were almost independent from the original noise level in the projections. Adaptive regularization was also obtained when changing the attenuation map and the background intensity with respect to the reference study, but strong structural changes in the activity distribution did not lead to optimal tradeoffs in terms of NMSE.

Adaptive regularization was demonstrated to be a practical way of modulating the level of filtering according to the noise present in the data in order to generate a more homogeneous image quality from patient to patient.

REFERENCES

- [1] R. J. Jaszczak, D. R. Gilland, M. W. Hanson, S. Jang, K. L. Greer, and R. E. Coleman, "Fast transmission CT for determining attenuation maps using a collimated line source, rotatable air-copper-lead attenuators, and fan-beam collimation," *J. Nucl. Med.*, vol. 34, pp. 1577–1586, 1993.
- [2] P. Tan, D. L. Bailey, S. R. Meikle, S. Eberl, R. R. Fulton, and B. F. Hutton, "A scanning line source for simultaneous emission and transmission measurements in SPECT," *J. Nucl. Med.*, vol. 34, pp. 1752–1760, 1993.
- [3] G. T. Gullberg, H. T. Morgan, G. S. L. Zeng, P. E. Christian, E. V. R. Di Bella, C. H. Tung, P. J. Maniawski, Y. L. Hsieh, and F. L. Datz, "The design and performance of a simultaneous transmission and emission tomography system," *IEEE Trans. Nucl. Sci.*, vol. 45, pp. 1676–1698, 1998.
- [4] E. P. Ficaro, J. A. Fessler, R. J. Ackerman, W. L. Rogers, J. R. Corbett, and M. Schwaiger, "Simultaneous transmission-emission Thallium-201 cardiac SPECT: Effect of attenuation correction on myocardial tracer distribution," *J. Nucl. Med.*, vol. 36, pp. 921–931, 1995.
- [5] E. P. Ficaro, J. A. Fessler, P. D. Shreve, J. N. Kritzman, P. A. Rose, and J. R. Corbett, "Simultaneous transmission/emission myocardial perfusion tomography: Diagnostic accuracy of attenuation-corrected 99mTc-Sestamibi single photon emission computed tomography," *Circulation*, vol. 93, pp. 463–473, 1996.
- [6] G. N. El Fakhri, I. Buvat, M. Péligrini, H. Benali, P. Almeida, B. Bendriem, A. Todd-Pokropek, and R. D. Paola, "Respective roles of scatter, attenuation, depth-dependent collimator response and finite spatial resolution in cardiac single-photon emission tomography quantitation: A Monte Carlo study," *Eur. J. Nucl. Med.*, vol. 26, pp. 437–446, 1999.
- [7] T. F. Budinger, G. T. Gullberg, and R. H. Huesman, *Emission Computed Tomography Image Reconstruction: From Implementation to Applications*, G. T. Herman, Ed. New York: Springer, 1979, pp. 147–246.
- [8] G. Demoment, "Image reconstruction and restoration: Overview of common estimation structures and problems," *IEEE Trans. Acoust., Speech, Signal Processing*, vol. 37, pp. 2024–2036, 1989.
- [9] L. T. Chang, "A method for attenuation correction in radionuclide computed tomography," *IEEE Trans. Nucl. Sci.*, vol. NS-25, pp. 638–643, 1978.
- [10] C. Riddell, B. Bendriem, M. H. Bourguignon, and J.-P. Kernevez, "Approximate inverse and conjugate gradient: Non symmetrical algorithms for fast attenuation correction in SPECT," *Phys. Med. Biol.*, vol. 40, pp. 269–281, 1995.
- [11] C. Riddell, A. Savi, M. C. Gilardi, and F. Fazio, "Frequency weighted least squares reconstruction of truncated transmission SPECT data," *IEEE Trans. Nucl. Sci.*, vol. 43, pp. 2292–2298, 1996.
- [12] M. G. Kang and A. K. Katsaggelos, "General choice of the regularization functional in regularized image-restoration," *IEEE Trans. Image Processing*, vol. 4, pp. 594–602, 1995.
- [13] L. Kaufman, "Maximum likelihood, least squares, and penalized least squares for PET," *IEEE Trans. Med. Imag.*, vol. 12, pp. 37–51, 1993.
- [14] I. G. Zubal, C. R. Harrell, and E. Smith, "Computerized 3D segmented human anatomy," *Med. Phys.*, vol. 21, pp. 299–302, 1994.
- [15] J. A. Fessler and W. L. Rogers, "Spatial resolution properties of penalized-likelihood image reconstruction: Space-invariant tomographs," *IEEE Trans. Image Processing*, vol. 5, pp. 1346–1358, 1996.